Stoichiometric network analysis of the oxalate–persulfate–silver oscillator

Bruce L. Clarke

Citation: The Journal of Chemical Physics **97**, 2459 (1992); doi: 10.1063/1.463084
View online: http://dx.doi.org/10.1063/1.463084
View Table of Contents: http://scitation.aip.org/content/aip/journal/jcp/97/4?ver=pdfcov
Published by the AIP Publishing

Stoichiometric network analysis of the oxalate–persulfate–silver oscillator

Bruce L. Clarke
Department of Chemistry, University of Alberta, Edmonton, Alberta, Canada T6G 2G2

(Received 4 March 1992; accepted 28 April 1992)

This paper illustrates an approach that can refine mechanisms and obtain information about rate constants from dynamical phase diagrams which show the regions of oscillation of a mechanism as a function of the experimental parameters. Possible mechanisms for the experimentally oscillating oxalate–persulfate–silver system are examined. Starting with a proposed mechanism by Ouyang and de Kepper, which they could not make oscillate, we show that some variations of the mechanism are stable for all nonnegative values of the rate constants. Other variations are unstable. For these variations, feedback cycles that lead to instability are compared with a conceptual picture of feedback in the experimental system. One unstable mechanism fits the picture well. Its unimportant reactions are omitted and an analytical solution for the unstable region using 13 adjustable parameters is obtained. The rate constants are adjusted to match this solution to the experimentally measured phase diagram. A good fit can only be obtained if $[O_2]$ is too low and k_1 is much smaller than the known value. Both discrepancies are resolved if Ag^{2+} oxidizes water. The analysis predicts the width of the unstable region can increase when more O_2 enters the reactor.

I. INTRODUCTION

For two decades, the author has believed that dynamical phase diagrams could be used as an extremely powerful tool for confirming reaction mechanisms and refining rate constants. The analysis presented here is the first time these techniques have succeeded in confirming a new mechanism by showing that the rate constants can be adjusted to make the dynamical phase diagram match the experimental phase diagram.

Dynamical phase diagrams are analogous to thermodynamic phase diagrams; however, instead of regions for solid, liquid, and gas, there are regions for stability, bistability, and oscillations. Instead of the temperature and pressure, the parameters are CSTR (continuously stirred tank reactor) flow rates and input concentrations. Every rate constant in the mechanism may be treated as a parameter. Thus, the experimentally measurable part of the phase diagram is actually a cross section through a much higher-dimensional phase diagram. In this paper, we calculate the full high-dimensional phase diagram analytically and then choose the rate constants to give a cross section that matches experiment.

The analogy between thermodynamic and dynamical phase diagrams helps explain why phase diagram regions are very sensitive to the small changes in the reaction mechanism. In a thermodynamic phase diagram, the liquid–gas coexistence curve is located where the attractive forces from the intermolecular potential generate a negative pressure that cancels the kinetic pressure. The kinetic pressure is the pressure an ideal gas would have at the liquid density, which can be 1000 times larger than the pressure on the phase coexistence curve. Since the location of the curve is determined by the cancellation of two large opposing pressures, small changes in the intermolecular potential can produce large shifts in the coexistence curve.

In a dynamical phase diagram, destabilizing feedback cycles are analogous to the attractive part of the intermolecular potential. Without them, the phase diagram would be stable everywhere. To produce instability, these cycles must overcome the stabilizing cycles that make thermodynamic equilibrium states stable. Thus, instability occurs when powerful destabilizing feedback cycles cancel powerful stabilizing cycles. The exact position of this balance on the dynamical phase diagram is extremely sensitive to the network and its rate constants. Minor modifications can eliminate the unstable region entirely.

This picture of the cancellation and the sensitivity of the phase diagram was discovered almost two decades ago.[1] I thought the sensitivity would prevent simple models such as the Oregonator[2] from matching experimental data. Recently, Ringland[3] calculated the dynamical phase diagram of a refined Oregonator called the Showalter–Noyes–Bar-Eli (SNB) model, and found extreme sensitivity to the parameters g and k_0. It differs very significantly from the experimental diagram even after two decades of refining the rate constants.

I once studied the Field–Noyes–Koros (FKN) mechanism[4] and proved stability for all positive rate constants. When Noyes suggested[5] that instability would occur if the oxidation of malonic acid stopped at formic acid instead of going completely to CO_2, I showed a modified FKN model has large regions of instability, but only at high formic acid concentrations[6,7] not reached in experiments. This is further evidence of the great sensitivity of the phase diagram to mechanistic details.

The approach that calculates phase diagrams is now called stoichiometric network analysis (SNA). Early phase diagrams[6–8] showed that certain species had to be at high or low concentration for instability and how certain pathways in the network produce instability through critical current cycles. However, the approach had one serious defect—only phase diagrams using special (**h**,**j**) parameters could be obtained. These could not be compared with experiments, where phase diagrams used CSTR flow rates and input species concentrations as parameters.

Today a "SNA computer program" calculates both types of phase diagrams. Point to point comparisons between exact diagrams in the "experimental parameters" and approximate diagrams in the (**h**,**j**) parameters will be made in this paper. They demonstrate that the mathematical approximations SNA uses to handle large networks work well.

II. THE OXALATE–PERSULFATE–SILVER (OPS) SYSTEM

The OPS system is particularly interesting for three reasons. First, it does not contain a halogen, as do almost all of the other nonenzymatic oscillators. Second, it has only oscillations and no region of bistability. Third, its mechanism is probably the most complex mechanism yet proposed for a chemical oscillator.

Oscillations in the OPS system were discovered by Ouyang.[9,10] The system consists of a CSTR into which oxalic acid, persulfate, and Ag^+ are injected at $pH \approx 1$. These solutions contain dissolved O_2 at various concentrations. The oscillations are followed using a platinum electrode and an oxygen sensitive electrode. Sinusoidal oscillations in dissolved O_2 and the electromotive force (emf) are observed. Figure 1 shows the experimental phase diagram replotted using a logarithmic scale. Note that oscillation occurs in a narrow band that is linear in a log–log plot. It moves to a higher flow rate when the persulfate input increases and to a lower flow rate when the oxalic acid input increases.

These experiments were run under conditions of excess persulfate. The persulfate cannot oscillate because too little oxalic acid is present to consume a significant fraction of the persulfate.

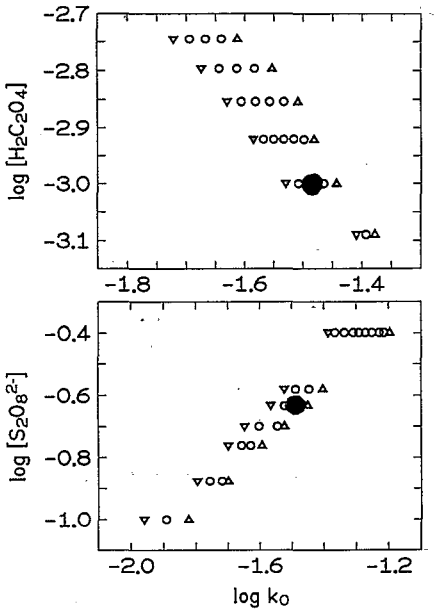

FIG. 1. Experimental phase diagram data replotted using a log scale. $[Ag_2SO_4]_0 = 5\times10^{-5}$ M, $[H_2SO_4]_0 = 5\times10^{-2}$ M. The large dot is a reference state which appears on many of the figures. In the reference state $k_0 = 3.25\times10^{-2}\,\mathrm{min}^{-1}$, $[H_2C_2O_4] = 1\times10^{-3}$ M and $[S_2O_8^{2-}] = 0.23$ M. The plot of log $[S_2O_8^{2-}]$ vs log k_0 is a cross section with $[H_2C_2O_4]$ at the reference state. The plot of log $[H_2C_2O_4]$ vs log k_0 is a cross section with $[S_2O_8^{2-}]$ at the reference state. Small circles denote experimental oscillations and triangles denote stable steady states.

Ouyang and de Kepper investigated the effect of varying O_2 concentrations in a series of batch experiments. Oxygen is a powerful inhibitor of the overall reaction, but oscillations can continue at various levels of dissolved oxygen. O_2 does not have a threshold level like Br^- in the Oregonator.

The mechanism they developed[9] is shown in Table I and is based on an earlier one by Kalb and Allen.[11] It is a radical chain mechanism where the chain initiation step R_1 was used by Kalb and Allen. Chain propagation steps R_2, R_3, R_4, and R_5 are identical to Kalb and Allen except for the inclusion of AgC_2O_4. They split the chain termination step of Kalb and Allen into $R_9 + R_{10}$ and introduced O_2 as an intermediate. This provides a way to explain the inhibitory effect of O_2.

Kalb and Allen explained rate law differences below and above $pH \approx 3\cdot5$ using Ag^{2+} and Ag, respectively. Ouyang's experiments[9] provide further evidence for Ag^{2+} at low pH.

Ouyang and de Kepper also introduced a second possible initiation step R_8 and new termination steps R_6, R_{11}, R_{16}, and R_{17}. They included steps that generate dissolved O_2 because of the effect of O_2 on the kinetics. They were unable to obtain oscillations in numerical simulations.

III. EQUATIONS FOR THE PHASE DIAGRAM

The objective in analyzing this mechanism is to find the source of the instability and rate constants that generate the experimental phase diagram. An outline of ideas which must be understood to follow the rest of this paper is given in the next three sections.

If the dynamics of the concentration vector **X** is expanded in a power series about a steady state $\mathbf{X}_0$ using $\Delta\mathbf{X} = \mathbf{X} - \mathbf{X}_0$,

$$\frac{d\Delta\mathbf{X}}{dt} = \mathsf{M}\Delta\mathbf{X} + \cdots, \tag{1}$$

the leading term M (the Jacobian) has the form

$$\mathsf{M} = \mathsf{N}\,\mathrm{diag}(\mathbf{v}_0)\mathsf{K}^t\,\mathrm{diag}(\mathbf{X}_0^{-1}). \tag{2}$$

M equals the stoichiometric matrix N times a matrix whose diagonal is the reaction rate vector $\mathbf{v}_0$ at steady state, times the transpose of the kinetic matrix K that gives the order of

TABLE I. Reaction mechanism of the oxalate–peroxydisulfate–silver oscillator.

(R_1)	$Ag^+ + S_2O_8^{2-} \rightarrow Ag^{2+} + SO_4^- + SO_4^{2-}$
(R_2)	$Ag^+ + SO_4^- \rightarrow Ag^{2+} + SO_4^{2-}$
(R_3)	$Ag^{2+} + C_2O_4^{2-} \rightleftharpoons Ag(C_2O_4)$
(R_4)	$Ag(C_2O_4) \rightarrow Ag^+ + CO_2^- + CO_2$
(R_5)	$CO_2^- + S_2O_8^{2-} \rightarrow CO_2 + SO_4^- + SO_4^{2-}$
(R_6)	$SO_4^- + H_2O \rightarrow OH + H^+ + SO_4^{2-}$
(R_7)	$H^+ + OH + O_2O_4^{2-} \rightarrow H_2O + CO_2^- + CO_2$
(R_8)	$Ag(C_2O_4) + S_2O_8^{2-} \rightarrow Ag^{2+} + CO_2^- + SO_4^- + CO_2 + SO_4^{2-}$
(R_9)	$CO_2^- + O_2 \rightleftharpoons O_2CO_2^-$
(R_{10})	$O_2CO_2^- + CO_2^- \rightarrow C_2O_4^{2-} + O_2$
(R_{11})	$Ag(C_2O_4) + CO_2^- \rightarrow Ag^+ + C_2O_4^{2-} + CO_2$
(R_{12})	$H^+ + CO_2^- + O_2 \rightarrow CO_2 + HO_2$
(R_{13})	$2HO_2 \rightarrow H_2O_2 + O_2$
(R_{14})	$2OH \rightarrow H_2O_2$
(R_{15})	$OH + H_2O_2 \rightarrow HO_2 + H_2O$
(R_{16})	$SO_4^- + CO_2^- \rightarrow SO_4^{2-} + CO_2$
(R_{17})	$Ag^{2+} + CO_2^- \rightarrow Ag^+ + CO_2$

kinetics of each species in each reaction, times a diagonal matrix of inverse steady state concentrations. This form of the Jacobian was the basis of a graph theoretical approach to stability analysis.[12] A general derivation is given in Ref. 13 [see Eq. (III.4) and (II.18) of Ref. 13].

If all eigenvalues of M are nonzero, the stability is determined by the eigenvalues. A point on a phase diagram corresponds to a particular value of a parameter vector **p**. Since M is a function of the parameters, varying **p** over the phase diagram varies M(**p**), its eigenvalues, and the stability.

A steady state is stable if all eigenvalues have negative real parts and unstable if any eigenvalue has a positive real part. Between these two simple cases, where the eigenvalues determine the stability, is a transition case where the stability is more difficult to determine. In this case, the eigenvalues have nonnegative real parts and some are zero.

The stable and unstable regions of the phase diagram are separated by hypersurfaces where the transition case occurs. When **p** crosses a transition hypersurface from a stable to an unstable region, some eigenvalues of M cross the imaginary axis from the left to the right side of the complex plane. When a single eigenvalue crosses the imaginary axis, a **saddle node bifurcation** occurs. When a pair of complex conjuate eigenvalues cross the imaginary axis, a **Hopf bifurcation** occurs.

The saddle node and Hopf bifurcation hypersurfaces determine the phase diagram. Mathematical equations for these hypersurfaces are obtained easily. The eigenvalues of M for a system with n intermediates are the roots λ of the characteristic equation

$$|\lambda \mathbf{I} - \mathsf{M}(\mathbf{p})| = \alpha_0 \lambda^n + \alpha_1(\mathbf{p})\lambda^{n-1} + \alpha_2(\mathbf{p})\lambda^{n-2} + \cdots + \alpha_n(\mathbf{p}) = 0, \tag{3}$$

where $\alpha_0 = 1$ by definition. If d is the rank of the stoichiometric matrix and $d \neq n$, the network has conservation conditions and these make the last $n - d$ characteristic equation coefficients vanish identically

$$\alpha_{d+1}(\mathbf{p}) = \alpha_{d+2}(\mathbf{p}) = \cdots = \alpha_n(\mathbf{p}) = 0.$$

The remaining coefficients $\alpha_1(\mathbf{p}),\ldots,\alpha_d(\mathbf{p})$ determine the phase diagram. On a saddle node bifurcation surface, one eigenvalue is zero. A root $\lambda = 0$ is possible if and only if $\alpha_d(\mathbf{p}) = 0$. Thus, all saddle node hypersurfaces in the phase diagram have the equation

$$\alpha_d(\mathbf{p}) = 0. \tag{4}$$

The Hopf bifurcation hypersurfaces can be described by exact and approximate equations. If $\alpha_i(\mathbf{p}) < 0$ for any $i = 1,\ldots,d$, the system is unstable. The region of the phase diagram obeying this condition lies inside the unstable region; however, the difference between this region and the exact unstable region is often negligible. In that case, the condition

$$\alpha_i(\mathbf{p}) = 0, \quad \text{for some } i < d \tag{5}$$

approximates the Hopf bifurcation hypersurface. This is the **α approximation.**

The exact conditions use the **Hurwitz determinants** Δ_i, $i = 1,\ldots,d$, which are defined as the $i \times i$ principal minors of the array

$$\begin{pmatrix} \alpha_1(\mathbf{p}) & \alpha_3(\mathbf{p}) & \alpha_5(\mathbf{p}) & \alpha_7(\mathbf{p}) & \cdots \\ \alpha_0(\mathbf{p}) & \alpha_2(\mathbf{p}) & \alpha_4(\mathbf{p}) & \alpha_6(\mathbf{p}) & \cdots \\ 0 & \alpha_1(\mathbf{p}) & \alpha_3(\mathbf{p}) & \alpha_5(\mathbf{p}) & \cdots \\ 0 & \alpha_0(\mathbf{p}) & \alpha_2(\mathbf{p}) & \alpha_4(\mathbf{p}) & \cdots \\ \cdots & \cdots & \cdots & \cdots & \cdots \end{pmatrix}. \tag{6}$$

Theorems[14] prove the eigenvalues of M are all in the left half of the complex plane if and only if

$$\Delta_i(\mathbf{p}) > 0, \quad i = 1,\ldots,d. \tag{7}$$

As **p** crosses a bifurcation surface from stable to unstable, condition (7) is violated crossing the transition hypersurface where one Δ_i becomes negative. Hence a bifuraction occurs on the hypersurface

$$\Delta_k(\mathbf{p}) = 0 \tag{8}$$

for some k.

To determine whether the bifurcation is a Hopf or saddle node, note that $\Delta_d = \alpha_d \times \Delta_{d-1}$. Saddle node bifurcations occur when a parameter change causes $\alpha_d(\mathbf{p})$ to change sign with all $\Delta_i > 0$ for $i = 1,\ldots,d-1$. On opposite sides of a saddle node bifurcation, $\Delta_d(\mathbf{p}) < 0$ and $\Delta_{d-1}(\mathbf{p}) > 0$.

All other bifurcations between stability and instability are Hopf bifurcations (provided only one pair of eigenvalues crosses the imaginary axis). The number of eigenvalues in the right half of the complex plane is determined by signs of the Δ_i's. A sign change in any Δ_k, $k < d$ when $\Delta_i > 0$ for all $i \neq k$, is a Hopf bifurcation.

IV. STATE PARAMETERS FOR CHEMICAL NETWORKS

A point on a thermodynamic phase diagram represents a set of thermodynamic state variables such a (T,P) or (T, V). The required number of variables depends on the number of components. A one-component system requires two variables for the phase diagram and three for the state.

Stoichiometric networks also have **complete sets of parameters.** One set is the rate constants **k** of all reactions in the network, plus constants **C** giving the concentrations of every conserved component. These will be called the (**k**,**C**) paramters. In the general network with n species, r reactions, and $d = \text{rank}(\mathsf{N})$, there are r **k**-type parameters and $n - d$ conservation constants. Hence the complete set has $r + n - d$ parameters. Reference 15 proves the dynamics of the intermediates is d dimensional and that these parameters specify completely the d-dimensional dynamical system.

The (**h**,**j**) parameters form another complete set. There are n **h**-type parameters and $(r - d)$ **j**-type parameters to make a total of $n + r - d$ parameters. (Every complete set has $n + r - d$ parameters.) The **j**-type parameters are the rates of $r - d$ extreme currents that must be chosen from f extreme currents.

Just as it is possible to plot a one-component thermodynamic phase diagram using any pair of intensive thermodynamic variables, a full dynamical phase diagram can use any complete set of parameters such as the (**k**,**C**) or (**h**,**j**) parameters. Just as fixing an extensive parameter does not affect a

thermodynamic phase diagram, fixing two extensive parameters does not affect the dynamical phase diagram. Fixing one **j** parameter sets the units used for the time scale and fixing one **h** parameter sets the units of concentration.

Only part of the phase diagram can be treated with any one set of $(r-d)$ extreme current parameters. The whole phase diagram must be broken up into regions where different sets of extreme currents are used.

The formula for M in terms of (**h**,**j**) parameters is obtained using $\mathbf{v}_0 = \mathsf{E}\mathbf{j}$ and $\mathbf{X}_0^{-1} = \mathbf{h}$ in Eq. (2)

$$\mathsf{M}(\mathbf{h},\mathbf{j}) = \mathsf{N}\,\mathrm{diag}(\mathsf{E}\mathbf{j})\mathsf{K}^t\,\mathrm{diag}(\mathbf{h}). \tag{9}$$

Since each element of M is linear in both **h** and **j**, the characteristic equation coefficients $\alpha_i(\mathbf{h},\mathbf{j})$ are polynomials of order i in both **h** and **j**. The Hurwitz determinants are polynomilas of order $i(i+1)/2$.

The signs of these polynomials and hence the stability are easy to determine in two situations. First, if all terms have positive coefficients, the polynomial is positive. This is a consequence of the (**h**,**j**) parameters being positive or zero. Second, if a polynomial contains negative terms, sometimes a single negative term can make the polynomial negative in some limit where the negative term becomes large. For example, the highest and lowest powers of x in $-x^5+x^4+x^3-x^2$ make the polynomial negative as $x\to\infty$ and $x\to 0$. When negative terms are present, this situation can be recognized using a simple test. The term is a **vertex of the exponent polytope**.

Polynomials that are difficult to treat because none of the negative terms are vertices of the exponent polytope have not been encountered in any network examined so far.

Approximate equations for the hypersurfaces of the phase diagram can be constructed by taking only a few dominant terms from these polynomials. The level of approximation corresponds to the edges (or one face), two faces,...,k faces of the exponent polytope.

V. APPROXIMATIONS USED BY SNA

SNA is an exact approach and simple mechanisms may be treated without any approximations. However, for large complex networks, approximations are necessary. This paper will examine the accuracy of the approximations used with the OPS system. Three kinds of approximations will be evaluated.

(1) **Current approximations.** A search for instability throughout all of parameter space requires $r-d$ of the **j**-type or **current parameters**. If k currents are used (**the k-current approximation**), only part of the parameter space will be examined. Instabilities can be missed. Instability in the halogen-based mechanisms can be detected using a one-current approximation.

(2) **The α approximation.** The Hopf bifurcation surface $\Delta_i(\mathbf{h},\mathbf{j})=0$ and the conditions for stability $\Delta_i(\mathbf{h},\mathbf{j})>0$ are approximated by similar conditions using $\alpha_i(\mathbf{h},\mathbf{j})$. A network is said to be α **stable** if all $\alpha_i>0$, and α **unstable** if any $\alpha_i<0$. Chemical oscillators examined to date are α unstable and the α approximation works well.

(3) **Exponent polytope approximations.** Hypersurfaces in the phase diagram are approximated using only those terms in the polynomial lying on a k-face of the exponent polytope. The simplest of this hierarchy of approximations is the edge approximation. It works well with all known chemical oscillators.

The α and exponent polytope approximations produce small errors in the locations of the phase diagram bifurcation curves.

VI. THE SEARCH FOR INSTABILITY AND OSCILLATIONS

The OPS network is quite stable and many attempts were made before finding instability. The first step in the analysis is to represent the mechanism as a diagram. The diagram notation completely specifies the stoichiometry, the orders of kinetics, which species are intermediates, and the species and pseudoreactions that represent the input or washing out of a species in the CSTR flow. Diagrams have many advantages. Since each species appears only once on the diagram, all reactions that produce or consume a given species can be identified quickly. Pathways and feedback loops are easily recognized.

The stability analysis software uses the reaction diagram as the definition of a network. To search for instability, the user sets up the reaction diagram on the computer screen and has the program do a stability analysis of the network represented by the diagram. It is simple to change the diagram and repeat the stability analysis.

Figure 2 shows the reaction diagram for all reactions in Table I except R_{16} and R_{17}. The convention of representing reactions with branched arrows and placing barbs and feathers on the branches to indicate stoichiometry and kinetics has been used many times before (see Refs. 6 and 13). Reversible reactions R_3 and R_9 are shown as double lines.

The diagram also shows which species are intermediates. Since reactions on the diagram do not have clearly defined left and right sides, and since SNA treats all nonnegative values of the rate constants so both directions of a reaction are equally important, the terms "reactant" and "product" are often ambiguous. Instead, nonintermediates will be called **major species**. The major species are marked on the diagram with cup-shaped **reservoir symbols**. This notation

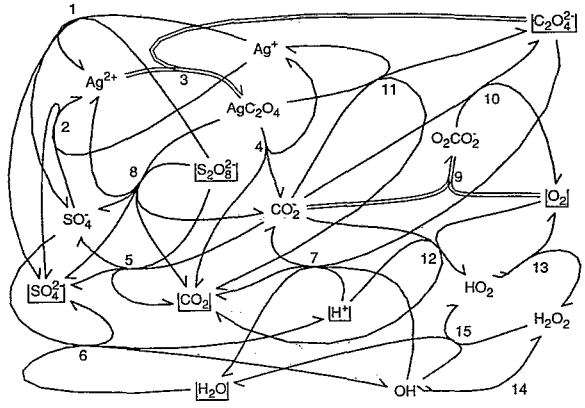

FIG. 2. Network diagram of Ouyang and de Kepper's mechanism in Table I.

conveys a picture of the species in a reservoir. The major species in Fig. 2 are $C_2O_4^{2-}$, $S_2O_4^{2-}$, SO_4^{2-}, CO_2, H_2O, H^+, and O_2. Field has devised a notation [see reaction (24) of Ref. 16] which conveys the same information when the mechanism is written using reactions. He places curly brackets around the major series. When R_8 is written in Field's notation

$$\mathrm{Ag(C_2O_4)} + \{\mathrm{S_2O_8^{2-}}\} \rightarrow \mathrm{Ag^{2+}} + \mathrm{CO_2^-} + \mathrm{SO_4^-} + \{\mathrm{CO_2}\} + \{\mathrm{SO_4^{2-}}\},$$

the reservoir symbols on the diagram become species with curly brackets.

Chain propagation shows up clearly in the upper left part of the diagram as a cycle involving Ag^{2+}, AgC_2O_4, CO_2^-, and SO_4^- via reactions R_2, R_3, R_4, and R_5. The initiation steps R_1 and R_8 produce species in the cycle. Oxalate is drawn into the cycle by R_3. The other reactions are mostly termination steps. Along the bottom of the diagram are the steps that lead to O_2 production.

The diagram shows that O_2 can affect the chain propagation via R_9 and R_{12} and thus influence its own production. To study whether feedback involving O_2 could produce instability, the network was modified so O_2 was an intermediate that exits the reactor. A search for instability using all one-current approximations found nothing. In the *BZ* system, one-current approximations always detect instability. Hence O_2 formation is probably not essential to the oscillation. This conclusion agrees with the experimental observation that oscillations occur for various O_2 concentrations. It does not have a threshold like Br^- in the *BZ* system.

Next, attention was focused on the chain reaction. Termination reactions R_{16} and R_{17} were added. Oxalate was changed from a major species whose concentration is fixed to an intermediate that enters via the CSTR flow. This change allowed oxalate to fluctuate and play a role in the feedback loops. Hurwitz determinants were calculated in the one-current approximation for every extreme current. No instability was found.

It now seemed unlikely that the mechanism could oscillate. Although modifications that produced instability could be invented, none had convincing chemistry. Work on this mechanism was abandoned and it became one of a large collection of mechanisms used for testing software.

One day while testing an algorithm that automatically searches for instability, I examined this mechanism after changing persulfate from a major species to an intermediate and including a pseudoreaction for persulfate entering in the CSTR flow. The one-current α approximation located instability for the extreme current in Fig. 3.

The destabilizing feedback cycle is given in Fig. 4. A positive feedback two cycle exists between persulfate and AgC_2O_4 because both are reactants of R_8. Another positive feedback two cycle exists between persulfate and Ag^+ because both are reactants of R_1. A positive feedback three cycle exists where AgC_2O_4 promotes Ag^+ via R_{11}, Ag^+ inhibits $S_2O_8^{2-}$ via R_1 and $S_2O_8^{2-}$ inhibits AgC_2O_4 via R_8. A positive feedback current cycle involving AgC_2O_4, $C_2O_4^{2-}$, R_3, and R_{11} also exists. The instability requires the participation of all four cycles and species. All are essential because if

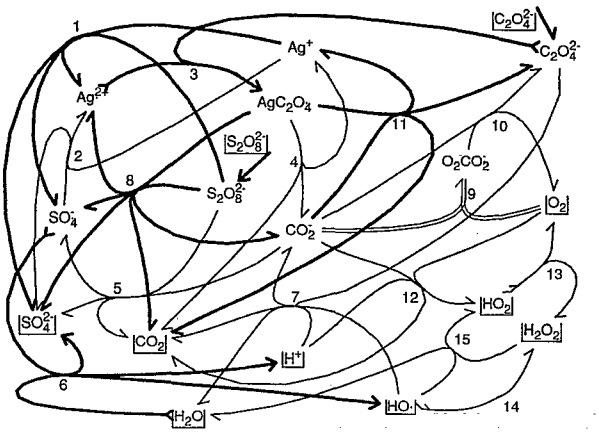

FIG. 3. Unstable extreme current of the modified network. Dark reactions are the extreme current. Light reactions belong to the underlying network and are not used by the current. (HO, HO_2, and H_2O_2 are major species so the stability analysis algorithms run faster.)

fewer were adequate, a destabilizing term would have occured in α_3. Destabilizing terms only occur in α_i for $i \geqslant 4$.

Eiswirth and Ross[17,18] have surveyed the main chemical oscillators and classified them according to the role of critical current cycles. This instability does not fit into their classification scheme. The destabilization is considerably more complex than in any other realistic oscillator.

The instability in the experimental system cannot be due to the feedback cycles of Fig. 4, where persulfate must fluctuate. Persulfate is in excess under experimental conditions and should not fluctuate.

VII. NEW SEARCH STRATEGY, NETWORK MODIFICATIONS

Even though instability shows up in the halogen oscillators using one-current approximations, such approximations do not show instability in the peroxidase enzyme system which Aguda and I studied.[19] We parametrized the unstable region using three currents and found that instability could not occur without a current where oxygen entered and was removed from the system. Since this current was stable by itself, instability required at least two currents. I

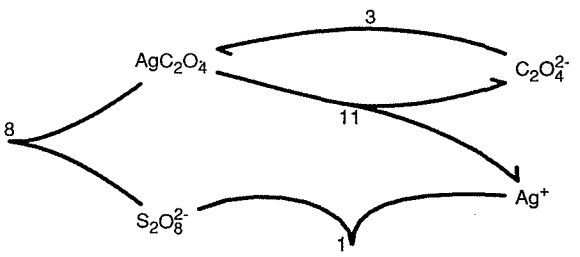

FIG. 4. Four positive feedback cycles combine to make the extreme current in Fig. 3 unstable. Mutual inhibition between reactants in R_8 produces a positive feedback two cycle between AgC_2O_4 and $S_2O_8^{2-}$. Inhibition between the reactants of R_1 produces another two-cycle between Ag^+ and $S_2O_4^{2-}$. There is also a current two cycle involving R_3 and R_{11} and another three cycle involving R_1, R_8, and R_{11}.

originally thought that this had something to do with the conservation condition for the enzyme and would not apply to nonenzyme networks. However, I began to wonder if the failure to detect instability in the OPS network could be due to the omission of currents such as oxalic acid entering and washing out of the reactor. These ideas lead to a new search strategy and the inclusion of more "exit reactions" in the mechanism.

In the α approximation when using k currents, α_i is a polynomial of order i in $n+k$ parameters. Since a $(k+1)$-current approximation has many more polynomial terms than a k-current approximation, it is computationally faster to test many k-current approximations than one $(k+1)$-current approximation.

A good strategy would be to make a random search of the interior of the current polytope using chords, then triangles,..., in an attempt to intersect the unstable region using as few currents as possible. Thus, we should examine all possible one-current approximations, then all possible two-current approximations,... . If a k-current approximation generates instability, higher-order current approximations containing this combination would be omitted. This is the **combinatorial search strategy**.

This strategy found a rich set of instabilities in the network OPSI shown in Fig. 5. Its unstable regions will be matched to the experiments in the latter sections of this paper. Several features of the network require discussion before continuing.

There are two kinds of major species. **Batch major species** are fixed like BrO_3^- in the *BZ* batch reactor. **CSTR major species** are like $C_2O_4^{2-}$ and $S_2O_8^{2-}$ in Fig. 3. These are major species inside the reservoir. They flow into the system where they become intermediates. CSTR major species are indicated in Figs. 3 and 5 by labeling the input pseudoreaction with the name of the species and a reservoir symbol. For these reactions, the software uses the CSTR flow rate k_0 as the rate constant.

In the network OPSI in Fig. 5, the CSTR input reaction for oxalic acid is reversible. This produces a current where oxalic acid enters and leaves the reactor. The network diagram shows $C_2O_4^{2-}$ because the ion is involved in the kinetics; however, at $pH \approx 1$, very little oxalic acid is oxalate. Because the acid hydrolysis is rapid, the dynamics and stability really depend on the combined concentrations of all forms of oxalic acid. In the stability analysis, the h parameter should be $1/[H_2C_2O_4]$. The rate constants that will make the phase diagram match experiments are based on rate laws for R_3 and R_7 which contain $[H_2C_2O_4]$. The true rate constants for R_3 and R_7 are $[H_2C_2O_4]/[C_2O_4^{2-}]$ times larger.

Oxygen is an intermediate which washes out of the CSTR. To simplify the preliminary analysis, I decided to omit the effects that O_2 might have on the chain reaction via R_9 and R_{12}. This makes O_2 a downstream product which cannot affect the stability. Oxygen is included so its steady state level can be compared with the experiments and O_2 oscillations simulated. To include oxygen while omitting the details of how it is formed, two new reactions are constructed

$$R_{67} = R_6 + R_7, \quad R_{18} = 4R_6 + R_{13} + R_{14} + 2R_{15}.$$

Also, reactions R_{11} and R_{16} of the original mechanism are equivalent to several other reactions

$$R_{11} = R_4 + R_9 + R_{10}, \quad R_{16} = R_6 + R_{12} + R_{13} + R_{15}.$$

Thus, when reactions R_{67}, R_{11}, R_{16}, and R_{18} are present, we can eliminate reactions R_6, R_7, R_9, R_{10}, R_{12}, R_{13}, R_{14}, and R_{15} from the network. The effect of O_2 on the chain reaction can be included by making O_2 a catalyst of R_{11} and R_{16}. This will be done later in this paper. Because O_2 has no effect on the stability, the entrance of oxygen into the CSTR was omitted from OPSI.

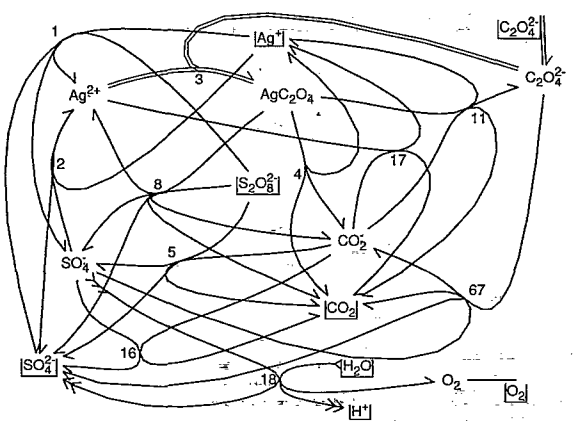

FIG. 5. The network OPSI. This network has all the features that produce instability in the experimental system. Note the numerous differences among this network, the stable network in Fig. 2, and the unstable but inapplicable network in Fig. 3.

VIII. STABILITY ANALYSIS OF OPSI

OPSI contains six intermediates ($n=6$), 15 reactions with reversible reactions counted twice ($r=15$), and no conservation conditions ($d=n=6$). A complete set of parameters uses $n+r-d=15$ parameters. The fact that OPSI is a CSTR and several reactions must have identical rate constants, k_0 will be taken into account later. For now, all 15 parameters are considered independent and nonnegative.

The first step is to calculate the extreme currents. The algorithm CORRALFRAME in Ref. 20 generated the extreme current matrix E in 26 s (see Ref. 21). It found $f=18$ currents, so E has 18 columns and 15 rows. Each extreme current is a possible pathway for the network's two overall reactions

$$S_2O_8^{2-} + C_2O_4^{2-} \rightarrow 2SO_4^{2-} + 2CO_2, \qquad (OVR_1)$$

$$4S_2O_8^{2-} + 2H_2O + 2C_2O_4^{2-} \rightarrow 8SO_4^{2-} + 4CO_2 + 4H + O_2. \qquad (OVR_2)$$

Every current has one of these overall reactions. Masuda[22] uses the term "reaction routes" to describe extreme currents when they are regarded as pathways for an overall reaction. The transpose of the current matrix is

E_1	0	0	1	1	0	0	0	0	0	0	0	0	0	0	0
E_2	0	0	0	0	0	0	0	0	0	0	0	0	1	1	0
E_3	0	1	1	0	1	1	0	0	0	0	0	0	1	0	0
E_4	1	1	2	0	1	0	0	0	1	0	0	0	1	0	0
E_5	1	0	1	0	1	0	0	0	0	1	0	0	1	0	0
E_6	1	1	1	0	1	0	0	0	0	0	1	0	1	0	0
E_7	0	0	0	0	0	1	1	0	0	0	0	0	1	0	0
E_8	0	1	2	0	0	0	0	1	1	0	0	0	1	0	0
E_9	0	0	1	0	0	0	0	1	0	1	0	0	1	0	0
E_{10}	0	1	1	0	0	0	0	1	0	0	1	0	1	0	0
E_{11}	1	0	1	0	0	0	1	0	1	0	0	0	1	0	0
E_{12}	1	0	0	0	0	0	1	0	0	0	1	0	1	0	0
E_{13}	2	0	2	0	2	2	0	0	0	0	0	1	2	0	1
E_{14}	4	0	4	0	2	0	0	0	2	0	0	1	2	0	1
E_{15}	4	0	2	0	2	0	0	0	0	0	2	1	2	0	1
E_{16}	0	0	2	0	0	2	0	2	0	0	0	1	2	0	1
E_{17}	2	0	4	0	0	0	0	2	2	0	0	1	2	0	1
E_{18}	2	0	2	0	0	0	0	2	0	0	2	1	2	0	1

The columns correspond to the reactions in the order R_1, R_2, R_3, R_{-3}, R_4, R_5, R_{67}, R_8, R_{11}, R_{16}, R_{17}, R_{18}, $H_2C_2O_4$ input, $H_2C_2O_4$ exit, and O_2 exit. Since currents having 0 in the right-hand column do not use the oxygen exit reaction, they do not produce O_2 and have overall reaction OVR_1. Those with a 1 in the right-hand column produce O_2 and have overall reaction OVR_2.

The combinatorial search strategy took one hour and 20 minutes to do a full algebraic stability analysis of all combinations of up to three currents. No single currents are unstable. There are 14 unstable pairs and four unstable triples that do not involve unstable pairs. The unstable pairs are 3–11, 4–7, 4–11, 4–12, 5–11, 6–11, 6–12, 7–8, 7–11, 8–11, 8–12, 9–11, 10–11, and 10–12. The triples are 3–7–9, 7–9–14, 7–9–17, and 7–10–17. (Here $i-j$ means $\mathbf{E}_i - \mathbf{E}_j$.)

To fit the unstable region to the data, the state (**h**,**j**) or (**k**, **C**) is placed in the unstable region and then parameters are adjusted to produce the correct phase diagram. To find the unstable region initially, I noted that most unstable current combinations involve currents $\mathbf{E}_{11}$ or $\mathbf{E}_7$. A stability analysis in the (**h**,**j**) parameters using these and several other currents produced a phase diagram in the (**h**,**j**) parameters which was displayed on the computer screen. The state (**h**,**j**) was placed in the middle of the unstable region.

The objective was to make a series of changes in the parameters so that (**h**,**j**) evolves into a point on the experimental phase diagram in the unstable region. During this evolution, the state (**h**,**j**) or (**k**,**C**) is kept unstable in order to determine which direction to adjust various parameters. An example will illustrate how the direction is determined. Suppose the CSTR flow rate k_0 must be decreased to match the experimental value and suppose k_0 cannot be decreased enough without leaving the unstable region. The strategy is to set k_0 to the flow rate at the lower edge of the unstable region and then examine another cross section through the steady state manifold such as k_1. Since the state is at the edge of the unstable region, it is also at the edge in the k_1 cross section. Moving k_1 into the interior of the unstable region and displaying the k_0 cross section again will show that the unstable region has shifted to a lower flow rate and the value of k_0 is now in the interior of the region. Thus k_0 can be decreased some more while keeping the state unstable.

This general method can be used to adjust any parameter in any direction keeping the state unstable. It was used to set the flow rate and the major species concentrations $[S_2O_8^{2-}]_0$, $[H_2C_2O_4]_0$, and $[Ag^+]$ to the experimental values. The same technique was used to make the upper and lower limits of the zone of instability in the flow rate match the experimental phase plot. In all, six parameters were determined by this data. In addition, the steady state concentrations of the six intermediates can be set to physically reasonable values. These 12 settings constrain the 15 parameters of the system. The three unconstrained degrees of freedom may be regarded as rates of negligible reactions which can be deleted.

IX. PARAMETER MANAGEMENT

Three issues will be addressed in this section. First, an algebraic stability analysis with all 15 parameters would be time consuming and unwieldly. I discuss how the least important reactions can be determined and how to check whether removing them affects the stability analysis. The second issue is how consistency is maintained between the (**h**,**j**) and (**k**,**C**) parameter systems. Finally, I discuss the requirement that several reactions have the same rate constant k_0 in a CSTR.

The number of currents required to treat r reactions is

$r-d$. If a reaction is deleted and the rank of the stoichiometric matrix d does not change, the state (**h**,**j**) requires one fewer current. Conversely, when a current is omitted and d does not change, one reaction is unused by the remaining currents. These currents represent a network with $r-1$ reactions. A simple rule to remember is "omitting a current is equivalent to omitting a reaction."

The initial stability analysis used only a few currents. It enabled me to place (**h**,**j**) in the unstable region; however, because too few currents were used, some reactions were unused. To put these back into the network, I changed all currents with $j_i = 0$ to $j_i = 1\times10^{-20}$. Including all currents ensured that all reactions were included. The stability of (**h**,**j**) was unaffected by these small currents.

The SNA computer program always makes sure the (**h**,**j**) and (**k**,**C**) parameters represent the same state. If the user changes (**h**,**j**), the program calculates matching (**k**,**C**) parameters using

$$\mathbf{k} = \mathrm{diag}(\mathsf{E}\mathbf{j})\mathbf{h}^{\mathsf{K}}.$$

(Since this network has no conservation conditions, **C** is not needed.)

If the user changes (**k**,**C**) the corresponding change in (**h**,**j**) is more difficult to calculate. The new **h** parameter is calculated from $\mathbf{h} = \mathbf{X}_0^{-1}$, and $\mathbf{X}_0$ is the solution of the system of nonlinear equations

$$\mathsf{N}\,\mathrm{diag}(\mathbf{k})\mathbf{X}_0^{\mathsf{K}} = 0.$$

The best way to solve these equations is to start with any known solution $\mathbf{X}_0^*$ for some rate constants $\mathbf{k}^*$. It can be obtained from any set of (**h**,**j**) parameters. Numerical continuation methods may be used to follow the solution as $\mathbf{k}^*$ changes into **k** and $\mathbf{X}_0^*$ changes into the desired solution $\mathbf{X}_0$.

The parameters are adjusted either by dragging (**k**,**C**) along the steady state manifold or by dragging (**h**,**j**) on the phase diagram. In each case, the software maintains correspondence between the parameters. Since it is important to know the extent of the unstable regions for both types of parameter adjustments, the stability of the steady state manifold is calculated by evaluating Δ_i, $i = 1,\ldots,d$ at each point.

Unstable regions due to $\alpha_d < 0$ are red on the (**h**,**j**) phase diagram and steady state manifold. The OPSI network has no negative terms in α_d so no red regions with saddle node bifurcations appear. When instability is caused by $\Delta_i < 0$, $i < d$, the phase diagram and steady state manifold are yellow, which indicates Hopf bifurcations. While adjusting the parameters, the colors enable the user to keep the state inside the unstable region on the (**h**,**j**) phase diagram or steady state manifold easily.

Both plots of the unstable region must correspond. The region on the steady state manifold is exact, while the region in the (**h**,**j**) phase diagram uses the analytical solution derived by making the α and edge approximations. The analytical solution is usually very close to the exact calculation.

Entrance and exit pseudoreactions for species in a CSTR all have the same rate constant k_0. When the software plots the steady state manifold vs k_0, it recognizes the CSTR reactions from the reaction diagram and ensures that all CSTR reactions have the same rate constants. When (**h**,**j**) parameters are calculated from the steady state manifold, they obey **the CSTR constraint**, which means all CSTR reactions have the same rate constant. However, on the (**h**,**j**) phase diagram, the user can set (**h**,**j**) to any values independently because they are independent in the stability analysis. Thus, the software must adopt special measures to allow the user as much freedom as possible to adjust (**h**,**j**) while still enforcing the CSTR constraint. Let us examine how the constraint can be enforced.

Suppose X is any intermediate which washes out of the CSTR using pseudoreaction R_i. Let exit(X) be the set of currents using R_i. Two expressions for the rate of the exit reaction R_i give the equation

$$k_0[\mathrm{X}] = \sum_{k\in \mathrm{exit}(X)} E_{ik} j_k.$$

If k_0 is given, the **h** parameter corresponding to X is

$$h_{\mathrm{X}} = \frac{1}{[\mathrm{X}]} = k_0 \Big/ \Big(\sum_{k\in \mathrm{exit(X)}} E_{ik} j_k \Big). \tag{10}$$

In a CSTR, the **h** parameters of exit species are determined by Eq. (10) and are dependent on the **j** parameters. If all species wash out of the reactor, every **h** parameter is dependent. Instead of $(n+r-d)$-independent (**h**,**j**) parameters, there are $(r-d)$ independent **j** parameters. There is no advantage in adding exit reactions to eliminate **h** parameters because at least as many new **j** parameters are required. In fact, negligible exit reactions should be omitted because a few more **h** parameters are easier to treat than many negligible exit currents.

The **h** parameter of one exit species can be made independent. This idea was exploited to make the inverse oxalic acid concentration h_{Ox} an independently adjustable parameter. The CSTR constraint for $H_2C_2O_4$ [Eq. (10)] involves only $\mathbf{E}_2$. It is

$$h_{\mathrm{Ox}} = k_0/j_2.$$

If h_{Ox} is taken as an independent parameter and k_0 is set to the desired flow rate, this equation determines j_2. However, the **j** parameters may all be rescaled to give the required j_2 without changing the phase diagram. Thus, h_{Ox} and k_0 may be adjusted independently if the $H_2C_2O_4$ CSTR constraint is satisfied by rescaling the **j**'s.

The concentration of $H_2C_2O_4$ in the feed is

$$[\mathrm{H_2C_2O_4}]_0 = \frac{\Sigma_{k\in S} E_{ik} j_k}{k_0}, \tag{11}$$

where S is the set of currents using the input pseudoreaction. Adjusting the parameter j_k for currents that consume oxalic acid modifies $[H_2C_2O_4]_0$. This must be kept fixed at the experimental value. To assist with this adjustment, the software displays the value of $[H_2C_2O_4]_0$ continuously as the parameters are changed.

X. ADJUSTING THE PARAMETERS

Numerous plots of phase diagrams and steady state manifolds were made while adjusting the parameters. Figure 6 shows a plot of log $[Ag^{2+}]$ vs log k_0. At this stage of adjustment, the state (**k**,**C**) is at the correct flow rate, but

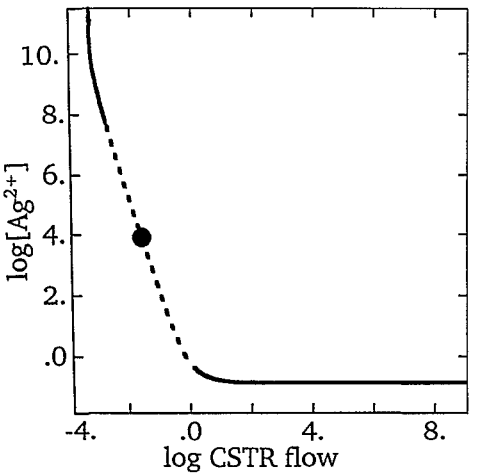

FIG. 6. The steady state of $[Ag^{2+}]$ as a function of the flow rate at one stage during the parameter adjustment. The dashed part of the curve is unstable. The dot represents the reference state shown on the experimental data in Fig. 1. Rate constants for this state are given in Table II under the heading OPSI[b].

$[Ag^{2+}]$ is absurdly high. The unstable region is orders of magnitude too wide.

The corresponding parameter point in the (**h,j**) phase plot appears in Fig. 7. The unstable region is long and narrow in qualitative agreement with experiments. The matching phase diagram of log $[H_2C_2O_4]$ vs log k_0 appears in Fig. 8. Figure 6 is a horizontal cross section through Fig. 8. The rate constants used for this and later phase diagrams are given in Table II.

The explosion of $[Ag^{2+}]$ occurs at low flow rates for all parameter values. Understanding this explosion is important. Silver(II) is produced by R_1 at a rate independent of the flow. In R_3, silver(II) reacts with oxalate which enters the system at a rate proportional to the flow. When the flow decreases, all entering oxalate is consumed by R_3 and the

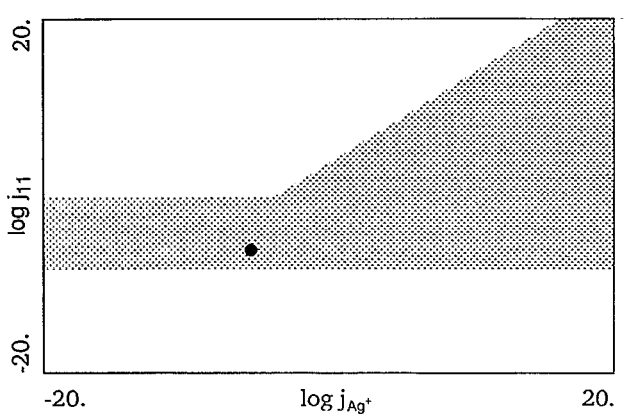

FIG. 7. The phase diagram in (**h,j**) for the OPSI[b] rate constants. The dot is the reference state. The vertical axis shows the flow in current E_{11}, which is the same as E_4 in the simplified OPSII network developed later. The lower edge of the shaded unstable region is a Hopf bifurcation curve, where instability only occurs when the current is above a threshold. This bifurcation curve has the same equation as the low-flow rate Hopf bifurcation in the experimental system. The horizontal axis is the flow of Ag^+ through the system.

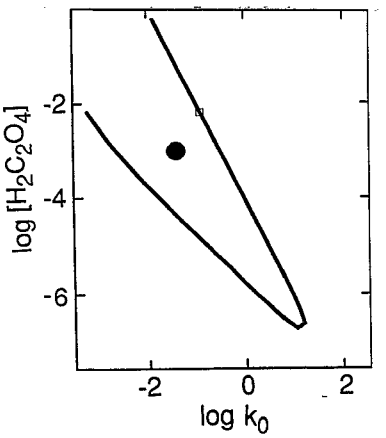

FIG. 8. The phase diagram of oxalic acid vs the flow rate for the OPSI rate constants. The dot is the reference state.

steady state $[H_2C_2O_4]$ falls to zero. If Ag^{2+} is produced by R_1 faster than oxalate is supplied, an explosion sends $[Ag^{2+}]$ to a mathematical infinity. This explosion can always be produced by lowering the flow rate. R_{17} cannot prevent the explosion by consuming the excess Ag^{2+} because it requires CO_2^-, and the only source of carbon in the system is oxalate. When oxalate is the limiting reagent, neither R_3 nor R_{17} can occur.

For all parameters, the unstable region occurs at a slightly higher flow rate than the $[Ag^{2+}]$ explosion. This

TABLE II. Parameters used to calculate the figures.[a]

Parameter	OPSI[b]	OPSI[c]	OPSII[d]
k_0	$3.018\,02\times10^{-2}$	$3.175\,97\times10^{-2}$	$3.251\,19\times10^{-2}$
$[H_2C_2O_4]_0$	$1.003\,68\times10^{-3}$	$1.003\,68\times10^{-3}$	$1.005\,36\times10^{-3}$
$[Ag^+]_0$	$1.006\,00\times10^{-4}$	...	...
k_1	0.353 252	$8.002\,04\times10^{-6}$	$1.048\,34\times10^{-2}$
k_2	$2.243\,97\times10^{9}$	$2.703\,89\times10^{8}$	...
k_3	5.839 23	5.839 25	$5.695\,32\times10^{7}$
k_{-3}	$1.032\,86\times10^{12}$	$1.032\,86\times10^{12}$	21.503 6
k_4	$1.529\,26\times10^{5}$	$3.980\,45\times10^{6}$	0.680 066
k_5	$2.664\,35\times10^{5}$	$2.664\,34\times10^{5}$	$1.423\,93\times10^{4}$
k_{67}	$1.866\,33\times10^{18}$	$1.866\,32\times10^{18}$	$4.570\,88\times10^{9}$
k_8	$1.680\,31\times10^{5}$	$1.680\,42\times10^{5}$	...
k_{11}	$4.811\,28\times10^{16}$	$4.811\,19\times10^{16}$	$4.000\,23\times10^{8}$
k_{16}	$6.503\,01\times10^{12}$	$6.499\,80\times10^{12}$	...
k_{17}	...	21.577 5	$1.359\,49\times10^{6}$
k_{18}	$1.452\,48\times10^{8}$	$1.452\,49\times10^{8}$	$1.834\,48\times10^{-2}$
$[H_2C_2O_4]$	$6.885\,58\times10^{-7}$	$1.821\,89\times10^{-4}$	$8.535\,48\times10^{-9}$
$[Ag^+]$	$1.229\,02\times10^{-5}$	$1.005\,99\times10^{-4}$ M	$1.005\,99\times10^{-4}$ M
$[S_2O_8^{2-}]$	0.230 00 M	0.230 00 M	0.230 00 M
$[Ag^{2+}]$	$9.174\,64\times10^{3}$	$5.384\,68\times10^{-3}$	$2.429\,10\times10^{-6}$
$[AgC_2O_4]$	$3.571\,40\times10^{-14}$	$5.546\,31\times10^{-18}$	$4.515\,61\times10^{-8}$
$[CO_2^-]$	$4.804\,94\times10^{-10}$	$4.257\,44\times10^{-10}$	$9.915\,52\times10^{-9}$
$[SO_4^-]$	$2.355\,01\times10^{-17}$	$7.267\,65\times10^{-20}$	$8.370\,02\times10^{-7}$
$[O_2]$	$2.881\,11\times10^{-9}$	$3.508\,99\times10^{-10}$	$4.722\,75\times10^{-7}$

[a] Rate constants and major species concentrations for the reference steady states (black dots) in the figures. All units are based on moles/liter and minutes. Major species concentrations are marked "M." Other concentrations are for steady state intermediates.

[b] These are the preliminary OPSI rate constants used in Figs. 6, 7, and 8.

[c] These are the final OPSI rate constants used in Fig. 9.

[d] The OPSII rate constants that give the phase diagrams in Figs. 13 and 14 that match the experiments.

region can be shifted to higher or lower flow rates by adjusting k_1. Hence, an approximate value for k_1 can be deduced by making the unstable region fall in the correct flow rate range.

Reducing k_1 shifts the explosion and unstable region to a lower flow rate. The unstable region becomes narrower. Increasing R_4 shifts the unstable region to a higher flow rate without affecting the width. Thus, reducing k_1 and increasing k_4 can narrow the unstable region without changing the flow rate. These ideas were used to match the flow rate range to the data when $[H_2C_2O_4]_0 = 1.0\times10^{-3}\,M^{-1}\,min^{-1}$. The resulting phase diagram is shown in Fig. 9.

This diagram is unsatisfactory because the width of the unstable region changes with the oxalic acid input. Also, many of the intermediate concentrations are too high (10^4) or low (10^{-20}). These cannot be adjusted easily to reasonable values by changing rate constants, but they can be adjusted easily by setting the (**h**,**j**) parameters on a phase diagram. To calculate a phase diagram, the number of **j** parameters should be reduced as much as possible by discarding negligible currents and reactions.

We now consider how the network could be simplified before calculating a phase diagram. The (**k**,**C**) phase diagram in Fig. 9 has a band of instability with a negative slope as in the experiments. This suggests the important reactions are correct and only the parameter values are wrong. We therefore simplify the network by keeping only the important reactions and currents used to calculate Fig. 9.

The currents of the reference state (**k**,**C**) in order from most important to least important are $\mathbf{E}_7$ $\mathbf{E}_2$, $\mathbf{E}_1$, $\mathbf{E}_{11}$, $\mathbf{E}_{12}$, $\mathbf{E}_{15}$, $\mathbf{E}_{18}$, $\mathbf{E}_{10}$ and $\mathbf{E}_9$. The rates of these nine currents range from 10^{-5} to 10^{-16}. Currents that are nine to 11 orders of magnitude smaller than the dominant currents can probably be discarded.

When (**k**,**C**) moves across the low flow rate Hopf bifurcation, the order of $\mathbf{E}_1$ and $\mathbf{E}_2$ change places. This suggests that the equation for the Hopf bifurcation is $j_1 = j_2$. Later we will obtain this equation from a stability analysis. When (**k**,**C**) moves across the high flow rate Hopf bifurcation, the sequence $\mathbf{E}_{12}\mathbf{E}_{15}$ changes to $\mathbf{E}_{15}\mathbf{E}_{14}$ and the order of the other currents remains the same.

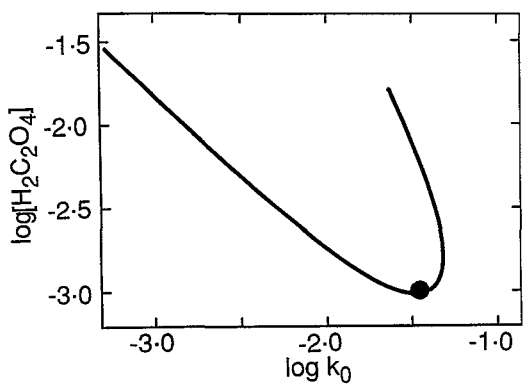

FIG. 9. The phase diagram for oxalic acid vs the flow rate for the final OPSI^c rate constants. Note that the range of instability for fixed $H_2C_2O_4$ is as narrow as in the experiments, but the narrowness occurs because the reference state is close to the tip of a parabola.

Since $\mathbf{E}_{15}$ is important and ranks sixth, the top six currents should all be retained in the stability analysis. To confirm this, I deleted the three least significant currents and calculated the steady state manifold showing the range of instability. No change was noticeable.

XI. ANALYSIS OF OPSII

The network OPSII (Fig. 10) is OPSI with reactions R_2, R_8, and R_{16} deleted. Only six currents are required in (**h**,**j**). Since all reactions are at least as fast as current $\mathbf{E}_{15}$ of OPSI, which determines the location of the Hopf bifurcation curve, this network is probably a minimal model which cannot be simplified further.

Silver(II) now generates O_2 via SO_4^- without a chain reaction. The extreme current matrix has eight currents. The columns of its transpose (below) are reactions R_1, R_3, R_{-3}, R_4, R_5, R_{67}, R_{11}, R_{17}, R_{18}, $H_2C_2O_4$ input, $H_2C_2O_4$ exit, and O_2 exit

$$\begin{array}{c} \\ \mathbf{E}_1 \\ \mathbf{E}_2 \\ \mathbf{E}_3 \\ \mathbf{E}_4 \\ \mathbf{E}_5 \\ \mathbf{E}_6 \\ \mathbf{E}_7 \\ \mathbf{E}_8 \end{array} \begin{pmatrix} 0 & 0 & 0 & 0 & 1 & 1 & 0 & 0 & 0 & 1 & 0 & 0 \\ 0 & 0 & 0 & 0 & 0 & 0 & 0 & 0 & 0 & 1 & 1 & 0 \\ 0 & 1 & 1 & 0 & 0 & 0 & 0 & 0 & 0 & 0 & 0 & 0 \\ 1 & 1 & 0 & 0 & 0 & 1 & 1 & 0 & 0 & 1 & 0 & 0 \\ 1 & 0 & 0 & 0 & 0 & 1 & 0 & 1 & 0 & 1 & 0 & 0 \\ 4 & 2 & 0 & 2 & 0 & 0 & 0 & 2 & 1 & 2 & 0 & 1 \\ 4 & 4 & 0 & 2 & 0 & 0 & 2 & 0 & 1 & 2 & 0 & 1 \\ 2 & 2 & 0 & 2 & 2 & 0 & 0 & 0 & 1 & 2 & 0 & 1 \end{pmatrix}.$$

The currents have been numbered, so the first six currents match the important currents of OPSI. They are in order of decreasing importance for the reference state. Currents $\mathbf{E}_1$ to $\mathbf{E}_8$ correspond to OPSI currents in the order $\mathbf{E}_7$, $\mathbf{E}_2$, $\mathbf{E}_1$, $\mathbf{E}_{11}$, $\mathbf{E}_{12}$, $\mathbf{E}_{15}$, $\mathbf{E}_{14}$ and $\mathbf{E}_{13}$. The other OPSI currents use R_2, R_8, or R_{16} and have no analogs in OPSII.

The current polytope is five-dimensional. Its geometry will tell us which six of the eight currents to use. It will also explain why current $\mathbf{E}_{12}$ of OPSI disappeared and $\mathbf{E}_{14}$ appeared crossing the Hopf bifurcation curve. The most signif-

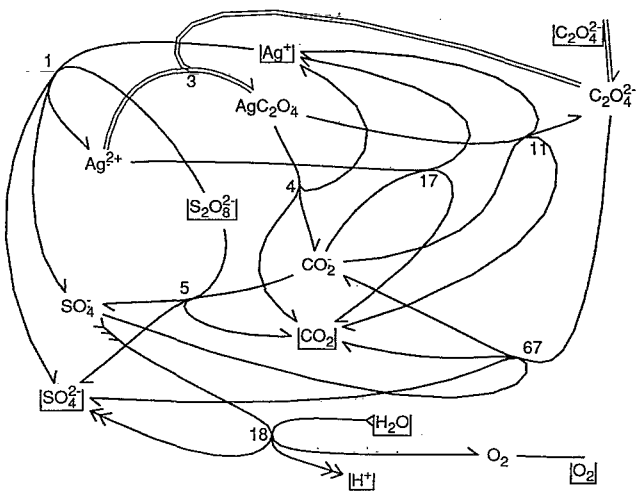

FIG. 10. The network OPSII, shown here, contains only the bare minimum that is necessary to produce a (**k**,**C**) phase plot matching the data.

icant feature of the current polytope is a three-dimensional face which is a rectangular prism (Fig. 11). The remaining two dimensions are built on this base by adding two more vertices (currents $\mathbf{E}_2$ and $\mathbf{E}_3$) which have edges connecting to every vertex of the prism. The entire polytope has eight vertices (currents).

To span the prism in a stability analysis, it is subdivided into three tetrahedra consisting of currents $\mathbf{E}_1$–$\mathbf{E}_4$–$\mathbf{E}_5$–$\mathbf{E}_6$, $\mathbf{E}_1$–$\mathbf{E}_4$–$\mathbf{E}_6$–$\mathbf{E}_7$, and $\mathbf{E}_1$–$\mathbf{E}_6$–$\mathbf{E}_7$–$\mathbf{E}_8$. Adding $\mathbf{E}_2$ and $\mathbf{E}_3$ to each of these produces three five-dimensional simplices S_1, S_2, and S_3 (respectively). A separate stability analysis is required for each simplex.

We can deduce *a priori* where instability will be found from the changes in the order of the currents crossing the Hopf bifurcation curves. Recall that crossing the high-flow Hopf bifurcation caused $\mathbf{E}_{12}$ to disappear and $\mathbf{E}_{14}$ to appear (in the numbering of OPSI). In the new numbering, $\mathbf{E}_5$ disappears and $\mathbf{E}_7$ appears. Geometrically, the state (**h**,**j**) moved roughly parallel to the diagonal between vertices 5 and 7. Thus, the state leaves simplex S_1 and enters simplex S_2 or S_3. The instability occurred in S_1.

A stability analysis using 12 parameters for simplex S_3 took 4 min and 34 s. The α_i polynomials have 2305 terms, which are all positive. S_3 is α-stable everywhere.

The analysis of S_1 produced 1369 terms with six negative vertices in α_4 and six in α_5. It took 85 min to convert the region of instability into 12 systems of inequalities with a total of 260 inequalities. The analysis of S_2 produced 2090 terms with four negative vertices in α_4 and eight in α_5. The analysis took 115 min to generate 12 systems with 272 inequalities in total. The inequality systems were saved so the (**h**,**j**) phase diagram could be displayed when needed without recalculation.

The (**h**,**j**) phase diagram makes it possible to set the intermediate concentrations directly. Because of the constraint that the state is in the unstable region, the most reasonable set of concentrations I could set was $[Ag^{2+}] = 2.4\times10^{-6}$, $[AgO_2O_4] = 2.5\times10^{-8}$, $CO_2^- = 1\times10^{-8}$, and $[SO_4^-] = 8.4\times10^{-7}$. It was not possible to make $[O_2]$ larger than about 4.8×10^{-7} M, which is far smaller than the 2.8×10^{-4} M reported by Ouyang and de Kepper. To maximize $[O_2]$, I maximized overall reaction (OVR_2) and reduced the importance of (OVR_1). This reduced the importance of R_{11}, R_{67}, and R_{17} and lowered the steady state concentrations of AgC_2O_4 and CO_2^-. The maximum $[O_2]$ production is achieved by maximizing $[SO_4^-]$, which then forms oxygen via R_{18}. These considerations explain why some concentrations are lower and higher.

XII. UNDERSTANDING THE STABILITY ANALYSIS

The inequalities may be interpreted to give a clear chemical understanding of the conditions for instability. This understanding is important when adjusting the parameters. The actual inequalities involve the logarithms of the (**h**,**j**) parameters, where j_i is the rate of $\mathbf{E}_i$ and h_i is $1/([X_i])$. For clarity, I will state the antilogarithmetic form of the inequalities and refer to concentrations.

The unstable region inside simplex S_1 is described by 260 inequalities. To find out which inequality is important when crossing the Hopf bifurcation curve at a particular point on the (**h**,**j**) phase diagram, I set up programming so clicking the mouse near the bifurcation curve displays the inequality. This makes it possible to focus attention on only the important inequalities.

Oxalic acid washes out of the system in only one current whose rate is j_2. In Fig. 9, this current was the largest contribution to the inflow of oxalic acid. Adjusting j_2 at fixed k_0 changes $[H_2C_2O_4]_0$ by Eq. (11). To keep this concentration fixed at the experimental value when changes in other currents affected the input of oxalic acid, I made minor adjustments in j_2 to restore the correct input rate. This approach worked until I tried to adjust the parameters to produce as much O_2 from oxalic acid as possible. Since less oxalic acid washes out, j_2 is smaller. It eventually becomes one of the least significant currents.

The entire region of instability is produced by the destabilizing feedback cycles in Fig. 12. One inequality system, which describes the requirements for instability in the experimentally applicable region, will be discussed in detail. Instability requires

$$j_1 > j_2, \tag{12}$$

which means the reversible cycling in the equilibrium of R_3 that forms AgC_2O_4 exceeds the flow of oxalic acid through the CSTR. A Hopf bifurcation occurs if j_2 increases and vio-

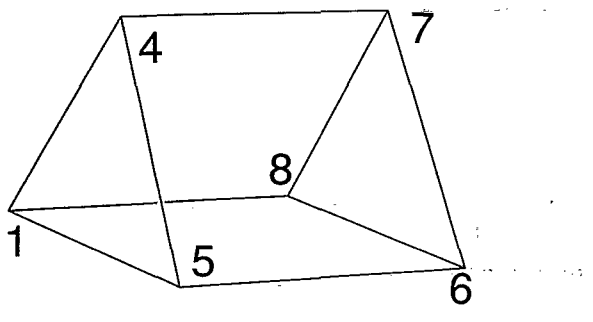

FIG. 11. One three face of the current polytope of OPSII. The unstable j parameter region is in the vicinity of vertices 1, 4, 5, and 6.

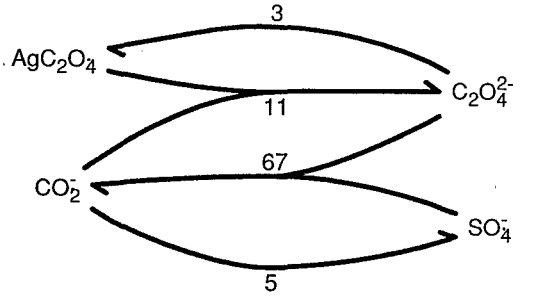

FIG. 12. The destabilization of OPSI involves four species and two positive two cycles. One cycle occurs when SO_4^- and $H_2C_2O_4$ react in R_{67} and the other occurs when Ag^{2+} and CO_2^- react in R_{17}. The first two cycle occurs in currents $\mathbf{E}_1$, $\mathbf{E}_4$, and $\mathbf{E}_5$, and the second in currents $\mathbf{E}_5$ and $\mathbf{E}_6$. The only current with both of these is $\mathbf{E}_5$, which is stable by itself.

lates this inequality. The Hopf bifurcation in Fig. 9 has the equation $j_1 = j_2$. Since that phase diagram has the wrong shape, I raised the reversible cycling in $R_3(j_1)$ so this inequality is satisfied by a wide margin. For my parameters, it does not produce Hopf bifurcation curves in the experimentally applicable region of the phase diagram.

Another requirement for instability is

$$j_4 > 6j_6. \tag{13}$$

Since $\mathbf{E}_6$ is the only current in simplex S_1 that produces O_2, I tried to maximize j_6 and therefore by Eq. (13) I had to maximize j_4. Since j_4 is part of the influx of oxalic acid, I made most of the influx contribute to j_4 rather than j_2. As I increased j_4, the instability moved to a lower flow rate because a larger fraction of the entering oxalic acid was reacting.

Instability also requires that

$$[Ag^{2+}] > [SO_4^-], \tag{14}$$

$$j_4[Ag^{2+}] > j_5[SO_4^-]. \tag{15}$$

These inequalities explain why the instability is closely associated with the Ag^{2+} explosion. If k_0 increases and $[Ag^{2+}]$ falls, these inequalities will be violated crossing the Hopf bifurcation on the high flow rate side of the oscillatory region. When I was adjusting the parameters to maximize O_2 production, I noted that $\mathbf{E}_5$ uses oxalic acid without producing O_2. Hence I made j_5 small. Then only the first of these inequalities is important. When I kept $[Ag^{2+}]$ fixed and gradually increased $[SO_4^-]$ until it equaled $[Ag^{2+}]$, the unstable region narrowed and eventually disappeared. This approach was used to adjust the width to match experiments. Then I adjusted j_4 to position the upper and lower Hopf bifurcation curves at the correct flow rate.

These adjustments were made while viewing the steady state manifold plotted against k_0 at a fixed oxalic acid input concentration. When the (**k**,**C**) phase diagrams were plotted (Figs. 13 and 14) the result was similar to the data in Fig. 1.

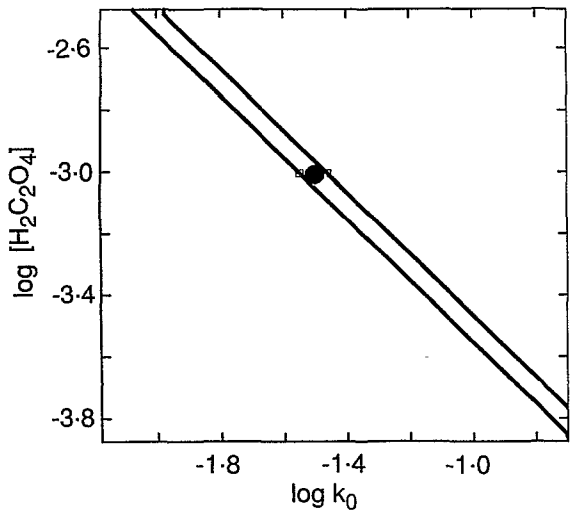

FIG. 13. The calculated phase diagram for oxalic acid vs the flow rate using the OPSII rate constants. The reference state and width of the unstable region match Fig. 1. This phase diagram was calculated using $\Delta_4 = \Delta_5 = 0$ and is exact. Equations (13) and (14) give the low flow and high flow Hopf bifurcation curves, respectively. These equations give a slightly wider zone of instability because of the edge approximation.

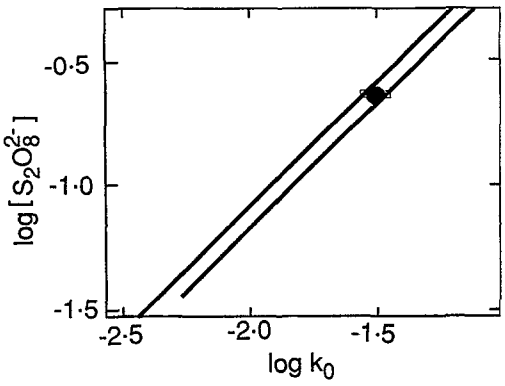

FIG. 14. The calculated phase diagram for persulfate vs the flow rate using the OPSII rate constants. The reference state and width of the unstable region match Fig. 1.

The error in the inequalities that were derived using the α and edge approximations can now be assessed. For $[H_2C_2O_4]_0 = 1.0\times10^{-3}$ M and $[S_2O_4^{2-}]_0 = 0.23$ M, the low-flow Hopf bifurcation occurs at $k_0 = 2.88\times10^{-2}$ M/min when calculated exactly using Δ_i, and at $k_0 = 6.6\times10^{-3}$ M/min on the (**h**,**j**) phase diagram where inequality (13) is an equality. The approximation is 4.4 times too low. The high-flow Hopf bifurcation occurs at $k_0 = 3.46\times10^{-2}$ M/min in the exact calculation and at $k_0 = 6.8\times10^{-2}$ M/min on the (**h**,**j**) phase diagram where inequality (14) is an equality. The approximation is two times too high.

The wider unstable region in the (**h**,**j**) phase diagram cannot be due to the α approximation, which always makes the unstable region appear too small. Probably all the error comes from the edge approximation. The unstable region comes from a single negative term in the 477-term polynomial α_4. Each inequality was obtained by throwing away all positive terms but one. The destabilizing term plus the stabilizing terms that give the upper and lower Hopf bifurcation curves in Figs. 13 and 14 are

$$\alpha_4 \approx \frac{j_1^2 j_3 j_4}{[Ag^{2+}][H_2C_2O_4][AgC_2O_4][CO_2^-]} + \frac{6j_1^2 j_3 j_6}{[SO_4^-][H_2C_2O_4][AgC_2O_4][CO_2^-]} - \frac{j_1^2 j_3 j_4}{[SO_4^-][H_2C_2O_4][AgC_2O_4][CO_2^-]}.$$

This equation is three vertices of the exponent polytope. Each positive term is joined by an edge to the negative term. Reference 23 explains the mathematics. Error factors of 2 and 4.4 in the bifurcation points are caused by leaving out positive terms from this polynomial. If the terms on two faces containing these edges were included, the unstable region would be slightly narrower and would probably match the exact calculations closely.

Very few of the inequalities are significant for a particular set of parameters. For the parameters in Figs. 13 and 14, the following inequalities are significant:

$$j_1 > 6j_6, \tag{16}$$

$$j_1[O_2] > j_6[H_2C_2O_4], \tag{17}$$

$$j_1[Ag^{2+}] > j_6[H_2C_2O_4], \tag{18}$$

$$j_1[Ag^{2+}] > 5j_6[CO_2^-], \tag{19}$$

$$j_4[Ag^{2+}] > j_6[AgC_2O_4]. \tag{20}$$

These might describe parts of the bifurcation curves which are not accessible experimentally.

XIII. THE EFFECT OF OXYGEN INFLUX

To investigate whether the concentration of O_2 in the input could affect the unstable region, I made the CSTR exit pseudoreaction for oxygen reversible. This introduced a new extreme current where O_2 enters and leaves the CSTR. Seven currents (13 parameters) are now required to represent (**h**,**j**) states of this network. Before O_2 can affect the unstable region, feedback must be included. Earlier we noted that reactions R_{11} and R_{16} allow oxygen to affect the radical chain, and only R_{11} used in OPSII. This reaction has two interpretations. It appears in the original network and is not affected by oxygen. However, it is also $R_4 + R_9 + R_{10}$. Step R_9 is first order in O_2. When R_{11} replaces these steps, it should be first order in O_2, which permits oxygen to affect Ag^{2+} directly. In the simplex S_1, this reaction is used only by E_4. A stability analysis of this network (which will be called OPSIII) was carried out in S_1 to determine whether the unstable region could be affected by O_2.

The analysis generated 452 inequalities in 4.6 h and produced almost exactly the same inequalities as in the previous section. However, if current E_4 is involved in the Hopf bifurcation, the width of the unstable region is narrower for low $[O_2]$. Since $h_{O_2} = 1/[O_2]$, when $[O_2]$ is small, h_{O_2} is large. Positive terms that can dominate at large h_{O_2} narrow the unstable region.

Oxygen effects occur when the high flow Hopf bifurcation is given by condition (15) instead of Eqs. (14), which occurs when $j_5 > j_1$. In that case, when oxygen falls below the threshold

$$[O_2] < j_6[SO_4^-]/j_4,$$

the unstable region may disappear completely, or it may exist and be narrower with the high-flow bifurcation being given by one of the inequalities

$$j_{O_2}[Ag^{2+}] > j_6[SO_4^-], \tag{21}$$

$$j_4[Ag^{2+}] > j_3[SO_4^-], \tag{22}$$

where j_{O_2} is the flow of oxygen through the system.

XIV. DISCUSSION

This study has shown that the parameters can be adjusted easily to give the correct phase diagram. Table II shows instability occurs at the reference state for three sets of rate constants that differ by many orders of magnitude. The rate constants were determined by the intermediate concentrations, which were given reasonable values to illustrate the approach for setting parameters. The resulting parameters should give roughly correct predictions for other properties of the system.

Figure 15 shows sinusoidal oscillations with a 61 min period for OPSII. The period was not considered while adjusting parameters. The experimental oscillations are sinusoidal and with periods in the range 22–80 min. At the reference state where this simulation was made, the period is 28 min.

Kalb and Allen[11] give $k_1 = 0.58\ M^{-1}\ min^{-1}$. Table II shows this is 55 times larger than the final value used for OPSII. None of the k_1 values in the table are as large and the closest value has an absurdly large $[Ag^{2+}]$. Large k_1 values make the rate of Ag^{2+} formation orders of magnitude larger than the flow of oxalic acid into the system. In the real system, the concentration of Ag^{2+} would not explode. Instead it would oxidize water by a step such as

$$Ag^{2+} + H_2O \rightarrow Ag^+ + H^+ + HO, \tag{R_{19}}$$

which is similar to the oxidation of water by SO_4^- in reaction (R_6). This new independent reaction generates new extreme currents with the overall reaction

$$2S_2O_8^{2-} + 2H_2O \rightarrow 4SO_4^{2-} + 4H^+ + O_2. \tag{OVR_3}$$

These currents are side reactions which affect the stability by altering the concentrations of Ag^{2+} and SO_4^-.

When the oxidation of water is included, O_2 is produced fast enough to give the O_2 concentrations observed in the experiments. With this new means of producing oxygen, extreme currents with overall reaction (OVR_1) could be more important. If current E_5 was important, inequality (15) could determine the Hopf bifurcation hypersurface and then the unstable region would be affected by O_2 input. When the concentration of O_2 in the feed increases, the zone of oscillation could increase in width and shift to a higher flow rate.

The new reaction (R_{19}) does not modify the picture of how instability occurs. When the flow rate k_0 is low enough, $[Ag^{2+}]$ is high. It does not matter whether the high value is the shoulder of an explosion or is limited by the oxidation of water. The high $[Ag^{2+}]$ makes the rate of O_2 formation by current E_6 large. The system is stable when j_6 is too large to satisfy one of the inequalities (13), (16), or (17). Starting in

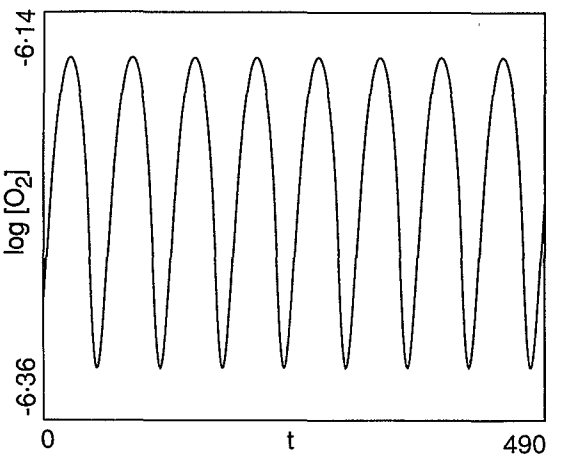

FIG. 15. Simulation of O_2 oscillations using the OPSII rate constants. The period is 61 min.

such a state, as the flow rate k_0 increases, $[Ag^{2+}]$ and j_6 decrease until these inequalities are all satisfied. This occurs at the low flow rate Hopf bifurcation point. As k_0 increases further, $[Ag^{2+}]$ decreases until one of inequalities (14), (15), (21), or (22) is violated. This occurs at the high flow rate Hopf bifurcation point.

The inequalities that give the conditions for oscillation are derived by the SNA program using symbolic algebra. This software makes it possible to do a similar analysis quickly and easily on most of the known experimental oscillators with mechanisms of similar complexity. This study taught us the importance of examining mixtures of currents when searching for instability. We learned that the α approximation works well, but the edge approximation can give error factors as large as 5. These errors are far smaller than the discrepancy Ringland found for the SNB model (Ref. 3) and are quite acceptable for exploratory work on mechanisms. SNA can give results to any desired accuracy using k-face approximations.

A thorough and complete quantitative analysis of the OPS system is feasible. Optimization of the phase diagram, using all known thermodynamic and rate constant data as constraints, would probably yield improved estimates of the rate constants. These developments will require software improvements to handle the extra parameters. The mathematical theory of how such an optimization can be carried out in the framework of SNA is being developed.

ACKNOWLEDGMENTS

The author would like to thank CNRS at Bordeaux, Patrick Hanusse, Patrick de Kepper, and Qi Ouyang for their hospitality and many discussions. Thanks are also extended to Weimin Jiang, Balder von Hohenbalken, and Baltz Aguda for code and algorithms used by the SNA program.

[1]B. L. Clarke, J. Chem. Phys. **58**, 5605 (1973).
[2]R. J. Field and R. M. Noyes, J. Chem. Phys. **60**, 1877 (1974).
[3]J. Ringland, J. Chem. Phys. **95**, 555 (1991).
[4]R. J. Field, E. Koros, and R. Noyes, J. Am. Chem. Soc. **94**, 8649 (1972).
[5]R. M. Noyes in *Faraday Symposia of the Chemical Society* (Chemical Society, London, 1974), No. 9, p. 79.
[6]B. L. Clarke, J. Chem. Phys. **64**, 4165 (1976).
[7]B. L. Clarke, J. Chem. Phys. **64**, 4179 (1976).
[8]B. L. Clarke, J. Chem. Phys. **60**, 1493 (1974).
[9]Q. Ouyang, Ph. D. thesis, University of Bordeaux, Bordeaux, France, 1987.
[10]Q. Ouyang and P. De Kepper, in *Spatial Inhomogenieties and Transient Behavior in Chemical Kinetics*, edited by P. Gray, G. Nicolis, F. Baras, P. Borckmans, and S. K. Scott (Manchester University, Manchester, England, 1990), p. 677.
[11]A. J. Kalb and T. L. Allen, J. Am. Chem. Soc. **86**, 5107 (1964).
[12]B. L. Clarke, J. Chem. Phys. **60**, 1481 (1974).
[13]B. L. Clarke, Adv. Chem. Phys. **43**, 1 (1980).
[14]F. R. Gantmacher, *Applications of the Theory of Matrices* (Interscience, New York, 1959).
[15]B. L. Clarke, J. Chem. Phys. **75**, 970 (1981).
[16]Y. X. Zhang and R. J. Field, J. Phys. Chem. **95**, 723 (1991).
[17]M. Eiswirth, A. Freund, and J. Ross, Adv. Chem. Phys. **80**, 127 (1991).
[18]M. Eiswirth, A. Freund, and J. Ross, J. Phys. Chem. **95**, 1294 (1991).
[19]B. D. Aguda and B. L. Clarke, J. Chem. Phys. **87**, 3461 (1987).
[20]B. von Hohenbalken, B. L. Clarke, and J. E. Lewis, J. Comp. Appl. Math **19**, 231 (1987).
[21]All calculation times in this paper are for a Compaq 386/20 PC running Microsoft OS/2 version 1.21. This machine has a speed rating of 0.12 MFLOPS (double precision LINPACK). Only 256 K of random access memory (RAM) storage was used during the symbolic algebra which generated polynomials and systems of inequalities.
[22]M. Masuda, J. Chem. Phys. **92**, 6030 (1990).
[23]B. L. Clarke, SIAM J. Appl. Math. **35**, 755 (1978).